Reaction Kinetics and Mechanism of Formation of $[MnMo_9O_{32}]^{6-}$ by Hypochlorous Acid Oxidation of $Mn^{2+}(aq)$ in the Presence of Molybdate†

Sarah J. Angus-Dunne,[a] Jenny A. Irwin,[a] Robert C. Burns,*[a] Geoffrey A. Lawrance[a] and Donald C. Craig[b]

[a] *Department of Chemistry, The University of Newcastle, Callaghan 2308, New South Wales, Australia*
[b] *Department of Chemistry, The University of New South Wales, Kensington 2033, New South Wales, Australia*

Oxidation of $Mn^{2+}(aq)$ by HOCl in weakly acidic solution, in the presence of molybdate, results in the formation of the soluble heteropolymolybdate $[MnMo_9O_{32}]^{6-}$. The speciation of Mn^{2+} in solution prior to oxidation has been examined using ESR spectroscopy and it has been established that the principal species is $[Mn(OH_2)_6]^{2+}$, there being evidence for weak interactions only with molybdate and isopolymolybdate anions. In keeping with this conclusion, the secondary manganese(II) polymolybdate species $Na_4[MnMo_8O_{27}]\cdot 20H_2O$ was crystallized from an acidic (pH 4.5) solution containing $Mn^{2+}(aq)$ and isopolymolybdate ions by slow vapour diffusion of ethanol into the aqueous phase. The compound crystallizes in the triclinic space group $P\bar{1}$, $a = 9.568(2)$, $b = 9.868(2)$, $c = 11.703(3)$ Å, $\alpha = 103.60(1)$, $\beta = 100.86(1)$ and $\gamma = 96.05(1)°$, and the structure was determined by X-ray diffraction methods to an R of 0.026 ($R' = 0.040$) for 3182 independent observed reflections. It consists of polymerized octamolybdate units linked through the sharing of common oxygen atoms and hydrated Mn^{2+} groups resulting in a sheet structure, with hydrated Na^+ ions also attached to the octamolybdate units. Uncomplexed water is also present. The kinetics of oxidation of Mn^{II} by HOCl was studied at 5–20 °C over the range pH 4.0–5.4 and found to exhibit solution autocatalytic behaviour. The oxidation kinetics followed the expanded rate expression $+d[MnMo_9O_{32}^{6-}]/dt = k_{AC}[Mn^{2+}][MnMo_9O_{32}^{6-}][HOCl]\cdot[MoO_4^{2-}][HMoO_4^-]$ based on an examination of [HOCl], pH and total $[MoO_4^{2-}]$ dependences, and arguments based on molybdate speciation under the reaction conditions. An approximate value of k_{AC} at 25 °C, $1.36(10) \times 10^8$ dm^{12} mol^{-4} s^{-1}, was estimated from an extrapolated value of the second-order autocatalytic rate constant using an Arrhenius plot and the reported formation constants describing the speciation of molybdate, isopolymolybdate and their protonated analogues in solution. A mechanism involving sequential one-electron oxidation steps of Mn^{2+} through to Mn^{4+} *via* Mn^{3+}, together with the equilibrium $Mn^{2+} + Mn^{4+} \rightleftharpoons 2Mn^{3+}$, which favours Mn^{2+} and Mn^{4+}, is able to account for the observed autocatalysis.

The oxidation of manganese(II) in aqueous solution has been the subject of numerous studies, and in many cases exhibits classical heterogeneous autocatalytic behaviour resulting from the formation of manganese dioxide.[1–5] In other instances $[MnO_4]^-$ can be found as a product in addition to MnO_2, as in the oxidation by iodate.[5] However, in the presence of molybdate under weakly acidic conditions, the soluble manganese(IV) heteropolymolybdate anion $[MnMo_9O_{32}]^{6-}$ is obtained rather than MnO_2 and there is no evidence for the formation of higher manganese oxidation states.[6,7] Recently, we reported the kinetics of oxidation of Mn^{II} in the presence of molybdate using peroxosulfate, HSO_5^-, at 40 °C and over a range pH 4.0–5.3 to give $[MnMo_9O_{32}]^{6-}$.[8] The kinetics exhibited non-linear dependences on both $[HSO_5^-]$ and $1/[H^+]$, while little influence on the rate constant was observed at pH 4.54 on varying the manganese to molybdenum ratio from 1:15 to 1:50. Subsequently, we examined the oxidation of Ni^{II} by peroxodisulfate, $S_2O_8^{2-}$, in the presence of molybdate at 80 °C over the range pH 3.0–5.2 to give the analogous nickel(IV) species $[NiMo_9O_{32}]^{6-}$.[9] In this case a linear dependence on oxidant was observed, and a non-linear dependence on $[H^+]$ involving a protonation–deprotonation equilibrium of the nickel(II) substrate species in solution, $[H_6NiMo_6O_{24}]^{4-}$. Again, little variation in the rate constant with Ni:Mo ratio was observed between 1:10 and 1:25 at pH 4.5. However, one significant difference between these two studies involved the dependences on $[H^+]$. In the case of the manganese system the observed rate constant decreased with increasing $[H^+]$, while in the nickel system the rate constant increased with increasing $[H^+]$. In view of this difference, using related oxidants and, supposedly, similar substrate species (*i.e.* $[H_6XMo_6O_{24}]^{4-}$, where X = Mn^{2+} or Ni^{2+}),[10] further studies into the more accessible manganese system were initiated. These involved an investigation into the speciation of Mn^{2+} in the presence of molybdate as well as further kinetic studies using HOCl and $S_2O_8^{2-}$ as oxidants. The results of some of these studies form the basis of the present work.

Experimental

Synthesis of $Na_4[MnMo_8O_{27}]\cdot 20H_2O$.—To a stirred solution containing $Na_2[MoO_4]\cdot 2H_2O$ (8.60 g, 35.5 mmol) in water (50 cm^3) was added a solution containing $MnSO_4\cdot H_2O$ (1.69 g, 10.0 mmol) in water (50 cm^3) followed by sufficient 0.5 mol dm^{-3} H_2SO_4 to adjust the pH to 4.5. The resulting pale yellow solution was transferred to a round-bottomed flask (250 cm^3) which was in turn placed inside a beaker (600 cm^3) containing ethanol (50 cm^3). The beaker was subsequently

† *Supplementary data available:* see Instructions for Authors, *J. Chem. Soc., Dalton Trans.*, 1993, Issue 1, pp. xxiii–xxviii.

covered with PARAFILM™ and the ethanol vapour allowed to diffuse into the aqueous solution. After 55 d at room temperature the pale yellow crystals that had formed were filtered off and dried under suction (3.03 g, 40%) (Found: Mn, 3.8; Mo, 44.3. $Na_4[MnMo_8O_{27}]\cdot 20H_2O$ requires Mn, 3.2; Mo, 45.0%). IR (CsI disc): 938s, 906s, 888s, 842m (Mo–O and Mn–O stretching), 669s (sh), 657s, 554s, 487m (sh) (Mo–O–Mo and Mo–O–Mn stretching), 353m and 288m (Mo–O–Mo and Mo–O–Mn bending) cm^{-1}.

Preparation and Standardization of HOCl.—Purified HOCl was obtained by vacuum distillation of an aqueous (400 cm^3) solution containing 15 g of calcium hypochlorite (30% minimum, AJAX, laboratory reagent) and 25 g of boric acid (BDH) at 40–50 °C. After rejecting the first 30–40 cm^3, about 300 cm^3 were collected. A nitrogen bleed was used to avoid excessive bumping. Using this procedure, aqueous solutions of approximately 0.1 mol dm^{-3} HOCl were obtained. The HOCl concentration was determined by iodometric titration using standardized $S_2O_3^{2-}$ of the mixture formed on addition of standard HCl (25 cm^3, 0.10 mol dm^{-3}) and KI (2 g) to HOCl (10 cm^3) in water (15 cm^3). The excess of acid was subsequently titrated against 0.10 mol dm^{-3} NaOH. Since HOCl and Cl_2 oxidize I^- with and without H^+ consumption, respectively, according to equations (1) and (2), the concentrations of HOCl

$$HOCl + 2I^- + H^+ \longrightarrow Cl^- + I_2 + H_2O \quad (1)$$

$$Cl_2 + 2I^- \longrightarrow 2Cl^- + I_2 \quad (2)$$

and Cl_2 may be calculated from these titres. From these results the amount of Cl_2 present was found to be always less than 1%.

Physical Methods.—Infrared spectra were recorded on a Bio-Rad FTS-7 Fourier-transform spectrophotometer fitted with CsI optics. Electron spin resonance spectra (X band) were obtained using a Bruker ESP300 spectrometer at a resonance frequency of 9600 MHz employing 100 kHz field modulation. A flat cell, as appropriate for aqueous solution, was employed and all measurements were made at room temperature. Samples were recorded using the same microwave power, scan rate and with the same number of scans to avoid spurious contributions to the linewidth and thereby allow direct comparison between spectra. Integrated intensities were based on the $m_I = +\frac{1}{2}$ hyperfine signal (see below) and were calculated assuming a Lorentzian lineshape using the expression (width)^2(height). This is only possible when there is evidence of a flat region between the individual hyperfine lines. In the very broadest signals there was little evidence of inflexion, and the errors associated with these measurements are consequently large. Microanalyses were carried out by the Analytical Unit at the Research School of Chemistry, Australian National University.

Kinetic Studies.—All reactions were monitored at 480 nm on a Hitachi 150-20 spectrophotometer with a thermostatted compartment stable to ±0.1 °C. Equal volumes of a buffered Mn^{2+}–$[MoO_4]^{2-}$ solution and a buffered HOCl solution, both of which had been pre-equilibrated to the appropriate temperature, were mixed in the cell to initiate the reaction. Final reaction mixtures, prepared in 0.5 mol dm^{-3} acetic acid–NaOH buffer solution, contained variable amounts of $MnSO_4\cdot H_2O$ (AJAX, AR grade) and $Na_2[MoO_4]\cdot 2H_2O$ (BDH, AR grade) as appropriate, with enough $NaNO_3$ (AJAX, AR grade) to yield a total ionic strength of 1.00 mol dm^{-3}. For the molybdate dependence, however, in order to obtain a wide range of Mn^{2+}:$[MoO_4]^{2-}$ ratios and high buffering capacity, solutions were prepared in 1.50 mol dm^{-3} acetic acid–NaOH buffer, and the final ionic strength was adjusted to 2.50 mol dm^{-3} using $NaNO_3$. Even so, some variation in pH (0.23 unit) was observed over the range of $[MoO_4]^{2-}$ concentrations used, although this proved no impediment to the analysis of the data.

Crystallography.—Crystal data. $Na_4[MnMo_8O_{27}]\cdot 20H_2O$, M = 1706.7, triclinic, space group $P\bar{1}$, a = 9.568(2), b = 9.868(2), c = 11.703(3) Å, α = 103.60(1), β = 100.86(1), γ = 96.05(1)°, U = 1041.7(4) Å^3, Z = 1, D_c = 2.72 g cm^{-3}, $F(000)$ = 821, λ(Mo-Kα) = 0.7107 Å, μ(Mo-Kα) = 27.18 cm^{-1}, crystal size 0.05 × 0.06 × 0.13 mm.

Data collection and processing. Reflection data were measured with an Enraf-Nonius CAD-4 diffractometer in θ–2θ scan mode using graphite-monochromated Mo-Kα radiation. Data were corrected for absorption by Gaussian integration using a 12 × 12 × 12 grid. A total of 3658 data were measured out to 2θ = 50°, giving a data set of 3182 reflections (minimum and maximum transmission factors 0.71 and 0.87) with $I > 3\sigma(I)$ after averaging, with R_{merge} = 0.010 for 205 pairs of equivalent $h0l$ reflections.

Structure determination. The structure was determined by Patterson and Fourier methods. Hydrogen atoms were not located. Positional and anisotropic thermal parameters for all atoms were refined using full-matrix least squares. Minor disorder was indicated by residual peaks in a Fourier difference map, which were interpreted as alternative positions for Na(2), O(W1) and O(W2). Site occupancies for the corresponding pairs of atoms refined to 0.75 [Na(2), O(W1) and O(W2)] and 0.25 [Na(2′), O(W1′) and O(W2′)]. A consequence of the disorder is that the Mn has two possible co-ordination octahedra, related by rotation of *ca.* 45° about the Mn–O(1). The water O(W8), which is bonded to Na(2) and Na(2′), has anomalous thermal motion, which probably indicates that it represents the overlap of two unresolved disordered atoms. Reflection weights used were $1/\sigma^2(F_o)$, with $\sigma(F_o)$ being derived from $\sigma(I_o) = [\sigma^2(I_o) + (0.04I_o)^2]^{\frac{1}{2}}$. The weighted residual is defined as $R' = (\Sigma w\Delta^2/\Sigma wF_o^2)^{\frac{1}{2}}$. Final R and R' values were 0.026 and 0.040, respectively. Atomic scattering factors and anomalous dispersion parameters were taken from ref. 11. Structure solution used parts of the MULTAN 80[12] package, and refinement used BLOCKLS, a local version of ORFLS.[13] The structural diagram was produced using ORTEP II[14] running on a Macintosh IIcx™, while an IBM 3090 computer was used for calculations.

The structure with atom numbering scheme is shown in Fig. 1. Atomic parameters and bond lengths and angles are given in Tables 1 and 2, respectively.

Additional material available from the Cambridge Crystallographic Data Centre comprises thermal parameters and remaining bond lengths and angles.

Results and Discussion

In our original kinetic studies of the formation of $[MnMo_9O_{32}]^{6-}$ by oxidation of Mn^{2+} in the presence of molybdate using peroxosulfate (HSO_5^-) as the oxidant[8] it was assumed that the Mn^{II} was present as $[H_6MnMo_6O_{24}]^{4-}$ or a closely related (*i.e.* differently protonated) species. This was based on the reported isolation of this compound in the solid state,[10] and the observed rate dependences and electrochemical results seemed consistent with this assumption.[8] Moreover, manganese(II) polymolybdate species could be isolated from solution over the range pH 3.5–5.5, and infrared examination of these materials indicated trends in the relative intensities of the M–O and O–H stretches which would be consistent with variation in protonation of the products. The colours of these materials also showed some variation, ranging from yellow-ochre at pH 5.5 to yellow at pH 3.5.

Some preliminary studies of the oxidation kinetics of Mn^{II} by HOCl in the presence of molybdate indicated that the system exhibited solution autocatalytic behaviour, as well as a molybdate dependence. This was markedly different to oxidation by peroxosulfate, which had shown non-linear dependences on $[HSO_5^-]$ and $1/[H^+]$ and no significant dependence on molybdate. This therefore prompted us to examine the speciation of Mn^{II} in acid solution in the presence

Table 1 Fractional atomic coordinates (non-hydrogen atoms) for $Na_4[MnMo_8O_{27}]\cdot 20H_2O$

Atom	*x*	*y*	*z*
Mn	0.000 0	0.000 0	0.500 0
Mo(1)	0.204 74(4)	0.116 58(4)	0.277 51(3)
Mo(2)	0.408 85(4)	−0.056 32(4)	0.115 72(3)
Mo(3)	0.148 56(4)	0.092 94(4)	−0.027 15(3)
Mo(4)	−0.074 72(4)	0.244 41(4)	0.152 62(3)
O(1)	0.102 7(3)	0.066 5(4)	0.373 2(3)
O(2)	0.120 5(3)	0.283 9(3)	0.251 7(3)
O(3)	0.018 5(3)	0.042 2(3)	0.121 0(3)
O(4)	0.295 0(3)	0.132 4(3)	0.116 7(3)
O(5)	0.262 8(3)	−0.059 6(3)	0.221 7(3)
O(6)	0.359 3(4)	0.212 2(4)	0.371 6(3)
O(7)	0.541 1(4)	0.023 0(4)	0.239 3(3)
O(8)	0.420 1(4)	−0.231 6(4)	0.090 7(3)
O(9)	0.500 0	0.000 0	0.000 0
O(10)	0.207 8(3)	−0.108 2(3)	−0.025 1(3)
O(11)	0.237 1(4)	0.128 7(4)	−0.132 0(3)
O(12)	0.061 9(3)	0.239 8(3)	0.008 5(3)
O(13)	−0.107 2(4)	0.402 8(4)	0.126 7(3)
O(14)	−0.157 2(4)	0.231 4(4)	0.268 3(3)
Na(1)	0.474 9(3)	−0.447 6(3)	0.144 6(3)
Na(2)	0.515 0(3)	0.341 6(4)	0.558 0(3)
O(W1)	−0.198 8(5)	0.064 0(6)	0.412 6(5)
O(W2)	0.062 7(5)	0.218 9(5)	0.615 4(4)
O(W3)	0.302 9(4)	−0.465 8(4)	0.267 4(4)
O(W4)	0.621 6(5)	−0.270 3(5)	0.316 9(6)
O(W5)	0.536 0(5)	−0.658 9(4)	0.183 1(4)
O(W6)	0.323 8(4)	−0.556 5(4)	−0.050 2(5)
O(W7)	0.603 8(4)	0.121 0(5)	0.562 6(4)
O(W8)	0.633 0(8)	0.427 1(10)	0.432 3(7)
O(W9)	0.089 8(4)	−0.304 8(4)	0.209 2(4)
O(W10)	0.104 8(5)	0.414 7(4)	0.491 4(3)
Na(2′)	−0.283 3(9)	0.179 6(9)	0.412 0(7)
O(W1′)	−0.041 3(17)	0.224 7(16)	0.561 2(14)
O(W2′)	0.206 5(15)	0.043 9(16)	0.625 9(13)

Primes indicate the minor (0.25) disorder component.

of molybdate and to look closely at the manganese(II) polymolybdate solids that could be isolated from solutions containing Mn^{2+} and molybdate over the range pH 3.5–5.5, in an attempt to isolate crystals suitable for X-ray examination.

In their original study, La Ginestra *et al.*[10] isolated a yellow-ochre material at pH 5.1 on mixing solutions of $MnSO_4$ and $[NH_4]_6[Mo_7O_{24}]$ (with a Mn : Mo ratio of 1 : 3.2), followed by overnight refrigeration. This product was characterized by chemical analysis (Mn, Mo and NH_3), infrared spectroscopy, X-ray powder diffraction, a magnetic measurement and a thermal gravimetric study. On this basis the product was formulated as $[NH_4]_4[H_6MnMo_6O_{24}]\cdot 3H_2O$, even though the infrared spectrum showed a marked difference to those of the other (similar) metal(II) heteropolymolybdates isolated in the same study, *i.e.* $[cation]_4[H_6MMo_6O_{24}]\cdot 5H_2O$, where cation = NH_4^+ or Na^+ and M^{II} = Co, Ni, Cu or Zn. Moreover, the X-powder diffraction pattern obtained suggests a somewhat different heavy-atom distribution in the structure compared to those of the other isomorphous species, notwithstanding the slight difference in the water of hydration.

Our extensive investigations of acidic Mn^{2+}–$[MoO_4]^{2-}$ solutions ultimately led to the isolation of yellow crystals from a solution of *ca.* pH 4.5 by slow vapour diffusion of ethanol into the aqueous phase, and proved to be $Na_4[MnMo_8O_{27}]\cdot 20H_2O$. In a formal sense, the formation of $[Mo_8O_{27}]^{6-}$ can be represented by the equation $8[MoO_4]^{2-} + 10H^+ \longrightarrow [Mo_8O_{27}]^{6-} + 5H_2O$, and the compound isolated contains this isopolymolybdate anion together with (hydrated) Na^+ and Mn^{2+} cations in the solid-state structure.

Crystal Structure of $Na_4[MnMo_8O_{27}]\cdot 20H_2O$.—The structure is based upon polymerized octamolybdate units which are linked through the sharing of common oxygen atoms and hydrated Mn^{2+} groups to produce a sheet structure, with hydrated Na^+ ions attached to the octamolybdate units. Also present are water molecules of crystallization. A view of one octamolybdate unit and its attendant hydrated Mn^{2+} and Na^+ ions is given in Fig. 1, showing the common oxygen atoms (with their attached molybdenum atoms) and Mn^{2+} linkages to adjacent octamolybdate units. A simple way to visualize the (idealized) octamolybdate unit is as a 'two-step' structure, with the lower step formed by Mo(1), O(4^I), Mo(2^I) and O(2), the upper step by Mo(2), O(2^I), Mo(1^I) and O(4), and the 'riser' between the steps by Mo(1), O(4), Mo(1^I) and O(4^I).

The octamolybdate unit sits at a centre of symmetry and is built up from distorted MoO_6 octahedra which share edges and, when linked to an adjacent unit or to an Mn^{2+} ion, an oxygen at a corner. The same type of configuration of eight shared MoO_6 octahedra is also found in the octamolybdate units of $[Mo_8O_{26}(OH)_2]^{6-}$, $[(HCO)_2Mo_8O_{28}]^{6-}$ and $[Mo_8O_{28}(MoO_3)_2]^{8-}$, all of which exist as discrete polymolybdate ions,[15–17] and also in the more closely related infinite chain of linked Mo_8O_{27} units found in $[NH_4]_6[Mo_8O_{27}]\cdot 4H_2O$.[18] In this latter example the octamolybdate units polymerize through the sharing of common oxygen atoms [corresponding to O(9) and O(9^I), as also found in the present structure!] to give the infinite chain, $(Mo_8O_{27}{}^{6-})_\infty$. The major difference between this latter structure and the present example are the additional linkages to different octamolybdate units through bridging *trans*-$Mn(OH_2)_4$ groups in $Na_4[MnMo_8O_{27}]\cdot 20H_2O$ [involving O(1) and O(1^I) of the octamolybdate unit], resulting in a sheet structure rather than an infinite chain.

Within the octamolybdate unit the Mo ··· Mo distances vary from 3.300 to 3.480 Å, and are comparable to those reported in $(Mo_8O_{27}{}^{6-})_\infty$ (3.258–3.472 Å). As expected, the Mo–O distances increase with increasing co-ordination of the oxygen atoms, disregarding co-ordination to either sodium or manganese, with average values of 1.708 (terminal oxygen), 1.964 (two-co-ordination), 2.107 (three-co-ordination) and 2.209 Å (four-co-ordination). Comparisons with the corresponding distances found in $(Mo_8O_{27}{}^{6-})_\infty$ are 1.713, 1.982, 2.112 and 2.190 Å, respectively. The unique feature of the present structure is the presence of an external, hydrated Mn^{2+} group, which also links adjacent octamolybdate units. The Mn^{II} is surrounded by an approximate square-planar arrangement of water molecules, exhibiting Mn–O distances (major water oxygen disorder component) of 2.211(5) and 2.213(5) Å, with the two remaining *trans* co-ordination sites occupied by oxygen atoms belonging to two separate octamolybdate units. These latter distances are 2.114(3) Å and are 16.8σ less than the average Mn–O(water) distance. The Mn–O(water) distances may be compared to those found in, for example, α-$MnCl_2\cdot 4H_2O$ [average 2.206(5) Å[19]] and $MnCl_2\cdot 2H_2O$ [2.150(5) Å[20]]. The two crystallographically unique sodium ions [with Na(2) exhibiting positional disorder] are each surrounded by five water molecules and an oxygen atom of an octamolybdate unit at distances of 2.272 Å upwards, to give an effective octahedral environment around each sodium.

A comment would appear appropriate with regard to the compound originally isolated by La Ginestra *et al.*,[10] which was formulated as $[NH_4]_4[H_6MnMo_6O_{24}]\cdot 3H_2O$. Comparison of the infrared spectra in the range 1000–700 cm^{-1}, which spans the Mo–O and Mn–O stretching regions, indicates that their material and $Na_4[MnMo_8O_{27}]\cdot 20H_2O$ are not the same. Some bands appear common to both spectra, but this is not surprising given the number and kind of metal–oxygen stretches expected to occur over the region involved. While the material obtained by La Ginestra *et al.* may contain some $Na_4[MnMo_8O_{27}]\cdot 20H_2O$, it is more likely to be a related compound containing an isopolymolybdate anion together with an external Mn^{2+}, that is a secondary heteropolymolybdate. Over the pH range used for the preparation of these species the isopolymolybdate anions which exist in solution are primarily $[Mo_7O_{24}]^{6-}$ and its

Table 2 Co-ordination geometries (bond lengths in Å, angles in °) around the molybdenums in the octamolybdate unit and around the Mn^{2+} and Na^{+} cations

For Mn with minor disorder components in square brackets

Mn–O(1)	2.114(3) [2.114(3)]	Mn–O(1^{II})	2.114(3) [2.114(3)]
Mn–O(W1)	2.211(5) [2.265(16)]	Mn–O($W1^{II}$)	2.211(5) [2.265(16)]
Mn–O(W2)	2.213(5) [2.164(14)]	Mn–O($W2^{II}$)	2.213(5) [2.164(14)]
O(1)–Mn–O(W1)	88.0(2) [87.3(4)]	O(W1)–Mn–O($W2^{II}$)	91.8(2) [87.6(6)]
O(1)–Mn–O(W2)	87.5(2) [89.2(4)]	O(W2)–Mn–O(1^{II})	92.5(2) [90.8(4)]
O(1)–Mn–O(1^{II})	180.0 [180.0]	O(W2)–Mn–O($W1^{II}$)	91.8(2) [87.6(6)]
O(1)–Mn–O($W1^{II}$)	92.0(2) [92.7(4)]	O(W2)–Mn–O($W2^{II}$)	180.0 [180.0]
O(1)–Mn–O($W2^{II}$)	92.5(2) [90.8(4)]	O(1^{II})–Mn–O($W1^{II}$)	88.0(2) [87.3(4)]
O(W1)–Mn–O(W2)	88.2(2) [92.4(6)]	O(1^{II})–Mn–O($W2^{II}$)	87.5(2) [89.2(4)]
O(W1)–Mn–O(1^{II})	92.0(2) [92.7(4)]	O($W1^{II}$)–Mn–O($W2^{II}$)	88.2(2) [92.4(6)]
O(W1)–Mn–O($W1^{II}$)	180.0 [180.0]		

For Mo(1)

Mo(1)–O(1)	1.739(3)	Mo(1)–O(4)	2.243(3)		
Mo(1)–O(2)	1.973(3)	Mo(1)–O(5)	1.888(3)		
Mo(1)–O(3)	2.221(3)	Mo(1)–O(6)	1.701(3)		
O(1)–Mo(1)–O(2)	100.0(1)	O(2)–Mo(1)–O(6)	94.3(1)		
O(1)–Mo(1)–O(3)	91.5(1)	O(3)–Mo(1)–O(4)	74.9(1)		
O(1)–Mo(1)–O(4)	164.3(1)	O(3)–Mo(1)–O(5)	85.8(1)		
O(1)–Mo(1)–O(5)	97.4(1)	O(3)–Mo(1)–O(6)	161.2(1)		
O(1)–Mo(1)–O(6)	104.3(2)	O(4)–Mo(1)–O(5)	74.3(1)		
O(2)–Mo(1)–O(3)	72.7(1)	O(4)–Mo(1)–O(6)	90.5(1)		
O(2)–Mo(1)–O(4)	83.5(1)	O(5)–Mo(1)–O(6)	101.9(1)		
O(2)–Mo(1)–O(5)	152.5(1)				

For Mo(2)

Mo(2)–O(4)	2.254(3)	Mo(2)–O(8)	1.704(3)		
Mo(2)–O(5)	2.039(3)	Mo(2)–O(9)	1.897(1)		
Mo(2)–O(7)	1.695(3)	Mo(2)–O(10)	2.208(3)		
O(4)–Mo(2)–O(5)	71.4(1)	O(5)–Mo(2)–O(1)	80.6(1)		
O(4)–Mo(2)–O(7)	96.0(2)	O(7)–Mo(2)–O(8)	104.8(2)		
O(4)–Mo(2)–O(8)	155.4(1)	O(7)–Mo(2)–O(9)	97.5(1)		
O(4)–Mo(2)–O(9)	86.3(1)	O(7)–Mo(2)–O(10)	163.8(2)		
O(4)–Mo(2)–O(10)	68.4(1)	O(8)–Mo(2)–O(9)	103.5(1)		
O(5)–Mo(2)–O(7)	90.2(1)	O(8)–Mo(2)–O(10)	89.4(2)		
O(5)–Mo(2)–O(8)	95.2(1)	O(9)–Mo(2)–O(10)	86.4(1)		
O(5)–Mo(2)–O(9)	157.2(1)				

For Mo(3)

Mo(3)–O(3)	2.428(3)	Mo(3)–O(11)	1.697(3)		
Mo(3)–O(4)	1.907(3)	Mo(3)–O(12)	1.750(3)		
Mo(3)–O(10)	2.125(3)	Mo(3)–O(3^{I})	1.934(3)		
O(3)–Mo(3)–O(4)	76.5(1)	O(4)–Mo(3)–O(3^{I})	142.3(1)		
O(3)–Mo(3)–O(10)	81.8(1)	O(10)–Mo(3)–O(11)	98.6(1)		
O(3)–Mo(3)–O(11)	179.1(1)	O(10)–Mo(3)–O(12)	158.1(1)		
O(3)–Mo(3)–O(12)	76.3(1)	O(10)–Mo(3)–O(3^{I})	74.8(1)		
O(3)–Mo(3)–O(3^{I})	75.5(1)	O(11)–Mo(3)–O(12)	103.2(2)		
O(4)–Mo(3)–O(10)	76.7(1)	O(11)–Mo(3)–O(3^{I})	103.9(1)		
O(4)–Mo(3)–O(11)	104.3(1)	O(12)–Mo(3)–O(3^{I})	98.1(1)		
O(4)–Mo(3)–O(12)	99.2(1)				

For Mo(4)

Mo(4)–O(2)	1.950(3)	Mo(4)–O(13)	1.710(3)		
Mo(4)–O(3)	2.251(3)	Mo(4)–O(14)	1.713(3)		
Mo(4)–O(12)	2.316(3)	Mo(4)–O(10^{I})	1.907(3)		
O(2)–Mo(4)–O(3)	72.4(1)	O(3)–Mo(4)–O(10^{I})	72.3(1)		
O(2)–Mo(4)–O(12)	78.5(1)	O(12)–Mo(4)–O(13)	84.1(2)		
O(2)–Mo(4)–O(13)	104.6(1)	O(12)–Mo(4)–O(14)	170.7(2)		
O(2)–Mo(4)–O(14)	95.0(1)	O(12)–Mo(4)–O(10^{I})	83.4(1)		
C(2)–Mo(4)–O(10^{I})	144.0(1)	O(13)–Mo(4)–O(14)	104.1(2)		
O(3)–Mo(4)–O(12)	70.5(1)	O(13)–Mo(4)–O(10^{I})	104.1(2)		
O(3)–Mo(4)–O(13)	154.5(2)	O(14)–Mo(4)–O(10^{I})	98.6(2)		
O(3)–Mo(4)–O(14)	101.4(2)				

For Na(1)

Na(1)–O(8)	2.441(4)	Na(1)–O(W4)	2.419(6)	Na(1)–O(W6)	2.392(5)
Na(1)–O(W3)	2.398(5)	Na(1)–O(W5)	2.344(5)	Na(1)–O($W6^{VI}$)	2.396(5)
O(8)–Na(1)–O(W3)	98.5(2)	O(W3)–Na(1)–O(W4)	86.6(2)	O(W4)–Na(1)–O(W6)	161.3(2)
O(8)–Na(1)–O(W4)	79.1(2)	O(W3)–Na(1)–O(W5)	85.8(2)	O(W4)–Na(1)–O($W6^{VI}$)	88.2(2)
O(8)–Na(1)–O(W5)	175.4(2)	O(W3)–Na(1)–O(W6)	99.7(2)	O(W5)–Na(1)–O(W6)	95.2(2)
O(8)–Na(1)–O(W6)	82.6(2)	O(W3)–Na(1)–O($W6^{VI}$)	169.2(2)	O(W5)–Na(1)–O($W6^{VI}$)	86.1(2)
O(8)–Na(1)–O($W6^{VI}$)	89.8(2)	O(W4)–Na(1)–O(W5)	102.8(2)	O(W6)–Na(1)–O($W6^{VI}$)	88.1(2)

For Na(2)

Na(2)–O(6)	2.382(4)	Na(2)–O(W8)	2.272(8)	Na(2)–O($W4^{VII}$)	2.314(7)
Na(2)–O(W7)	2.427(5)	Na(2)–O($W3^{VII}$)	2.396(5)	Na(2)–O($W8^{VIII}$)	2.801(12)
O(6)–Na(2)–O(W7)	85.7(2)	O(W7)–Na(2)–O(W8)	103.8(3)	O(W8)–Na(2)–O($W4^{VII}$)	174.1(3)
O(6)–Na(2)–O(W8)	81.7(2)	O(W7)–Na(2)–O($W3^{VII}$)	91.0(2)	O(W8)–Na(2)–O($W8^{VIII}$)	86.7(4)
O(6)–Na(2)–O($W3^{VII}$)	172.5(2)	O(W7)–Na(2)–O($W4^{VII}$)	81.8(2)	O($W3^{VII}$)–Na(2)–O($W4^{VII}$)	89.1(2)
O(6)–Na(2)–O($W4^{VII}$)	97.1(2)	O(W7)–Na(2)–O($W8^{VIII}$)	168.8(2)	O($W3^{VII}$)–Na(2)–O($W8^{VIII}$)	92.5(2)
O(6)–Na(2)–O($W8^{VIII}$)	92.0(2)	O(W8)–Na(2)–O($W3^{VII}$)	92.5(2)	O($W4^{VII}$)–Na(2)–O($W8^{VIII}$)	87.6(2)

For Na(2′)

Na(2′)–O(14)	2.362(9)	Na(2′)–O($W7^{V}$)	2.382(9)	Na(2′)–O(W1′)	2.550(18)
Na(2′)–O(7^{V})	2.450(9)	Na(2′)–O($W8^{V}$)	2.622(14)	Na(2′)–O($W2'^{II}$)	2.368(17)
O(14)–Na(2′)–O(7^{V})	85.8(3)	O(7^{V})–Na(2′)–O($W7^{V}$)	96.1(3)	O($W7^{V}$)–Na(2′)–O(W1′)	88.6(5)
O(14)–Na(2′)–O($W7^{V}$)	176.0(4)	O(7^{V})–Na(2′)–O($W8^{V}$)	104.3(3)	O($W7^{V}$)–Na(2′)–O($W2'^{II}$)	89.9(4)
O(14)–Na(2′)–O($W8^{V}$)	87.7(3)	O(7^{V})–Na(2′)–O(W1′)	149.3(5)	O($W8^{V}$)–Na(2′)–O(W1′)	105.4(5)
O(14)–Na(2′)–O(W1′)	88.0(4)	O(7^{V})–Na(2′)–O($W2'^{II}$)	72.7(4)	O($W8^{V}$)–Na(2′)–O($W2'^{II}$)	174.4(5)
O(14)–Na(2′)–O($W2'^{II}$)	87.3(4)	O($W7^{V}$)–Na(2′)–O($W8^{V}$)	95.2(3)	O(W1′)–Na(2′)–O($W2'^{II}$)	77.1(5)

Symmetry codes: I $-x, -y, -z$; II $-x, -y, 1-z$; V $x-1, y, z$; VI $1-x, -1-y, -z$; VII $1-x, -y, 1-z$; VIII $1-x, 1-y, 1-z$. Primes indicate the minor (0.25) disorder component.

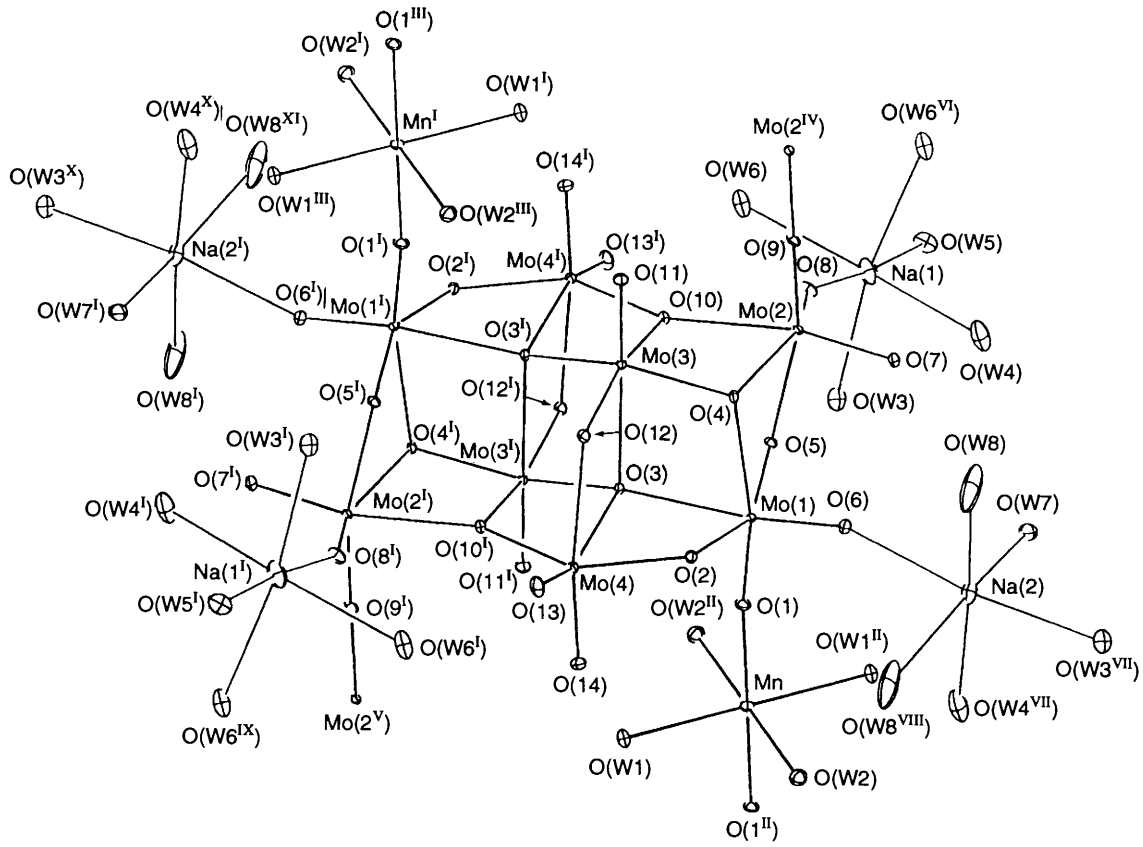

Fig. 1 View of the octamolybdate unit with attendant co-ordinated hydrated Mn^{2+} and Na^+ ions. Symmetry operations used in the diagram are: I $-x, -y, -z$; II $-x, -y, 1-z$; III $x, y, z-1$; IV $1-x, -y, -z$; V $x-1, y, z$; VI $1-x, -1-y, -z$; VII $1-x, -y, 1-z$; VIII $1-x, 1-y, 1-z$; IX $x-1, 1+y, z$; X $-1-x, y, z-1$; XI $x-1, y-1, z-1$

protonated form. However, other isopolymolybdates have been isolated from both aqueous and non-aqueous solution and include $[Mo_6O_{19}]^{2-}$, α- and β-$[Mo_8O_{26}]^{4-}$, $[HMo_5O_{17}]^{3-}$ and, as indicated above, the polymeric $(Mo_8O_{27}^{6-})_\infty$.[21] These generally appear to be stable only in the solid state. Thus, the original material isolated by La Ginestra *et al.* may contain a mixture of isopolymolybdate anions, or even a currently unrecognized species such as '$Mo_6O_{21}^{6-}$'* (based on the observed NH_4^+ : Mn : Mo ratios). If, as suggested, Mn^{II} does not exist as a primary heteropolymolybdate with the Anderson structure,[21] this is probably related to the size of the Mn^{2+} ion. All of the other divalent first-row transition metals which are reported to be central ions in this structure, *i.e.* [cation]$_4$[$H_6MMo_6O_{24}$]·$5H_2O$, where cation = NH_4^+ or Na^+ and M^{II} = Co to Zn, have smaller ionic radii than Mn^{2+}, and it may be that this type of geometry cannot enclose an ion the size of Mn^{2+} within the octahedral cavity at the core of the structure.

Speciation of Mn^{2+} *in the Presence of Molybdate.*—In order to establish the nature of Mn^{2+} in aqueous solution in the presence of molybdate and acetate buffer in conjunction with a study of the oxidation kinetics of formation of $[MnMo_9O_{32}]^{6-}$ with HOCl as oxidant, ESR spectroscopy was used to investigate solutions of the actual composition employed in that study.

The ESR spectra of Mn^{2+} (0.0025 mol dm^{-3}) in (*a*) aqueous solution at pH 5.3, (*b*) aqueous solution at pH 5.3 with added molybdate (0.0625 mol dm^{-3}) and $NaNO_3$ such that I = 1.00 mol dm^{-3}, (*c*) acetate buffer at pH 5.3 (I = 1.00 mol dm^{-3}) and (*d*) acetate buffer and added molybdate (0.0625 mol dm^{-3}) at pH 5.3 (I = 1.00 mol dm^{-3}) were investigated. The relevant data for g_{av}, A_{iso}, linewidth (for $\Delta m_I = +\frac{1}{2}$) and relative integrated intensity are given in Table 3. All of the spectra consist of a typical six-line pattern indicating coupling with the ^{55}Mn nuclear spin ($I = \frac{5}{2}$, 100% abundant). For Mn^{2+}, the $3d^5$ electron configuration ($S = \frac{5}{2}$) coupled with the nuclear spin actually gives rise to 36 energy levels in a magnetic field, resulting in 30 allowed transitions ($\Delta m_S = 1$ and $\Delta m_I = 0$). The six resolved lines correspond to the six orientations of the nuclear magnetic moment ($\Delta m_I = +\frac{5}{2}$ to $-\frac{5}{2}$), so that each line really consists of five unresolved transitions with $\Delta m_S = 1$. Splitting of this fine structure occurs because of a second- (and fourth-) order effect in the electron–nuclear hyperfine interaction which is field dependent, leading to linewidth variations for the six resolved Δm_I transitions.[22] Of these, the fourth line ($\Delta m_I = +\frac{1}{2}$) from the low-field end of the spectrum is the least affected, and this is used in studies (including this work) relating to relaxation and the effect of ligand substitution on the ESR signal of solvated Mn^{2+}.[23,24]

Now, whether or not an ESR signal is observed in solution depends on the linewidth, which in turn relies on the extent of zero-field splitting for the Mn^{2+} environment. For octahedrally co-ordinated Mn^{2+}, such as $[Mn(OH_2)_6]^{2+}$, a static zero-field splitting is necessarily absent, and relaxation in solution has been attributed to a fluctuating zero-field splitting caused by distortions of the octahedral geometry of the hydrated ion through collisions with other water molecules.[25] In the presence of ligands like Cl^- and SO_4^{2-}, which have low first formation constants ($K_1 \approx 1$ and 3.7 dm^3 mol^{-1}, respectively, at 25 °C and I = 1.0 mol dm^{-3})[26] for their $[Mn(OH_2)_5L]^{n+}$ species (L = Cl^- or SO_4^{2-}), some broadening is observed relative to $[Mn(OH_2)_6]^{2+}$.[23] This is again attributable to fluctuating zero-

* The hypothetical $[Mo_6O_{21}]^{6-}$ species may be obtained from $[Mo_8O_{27}]^{6-}$ by shortening the length of the 'steps', for example, by removing the two molybdate units built around Mo(1) and Mo(2) and subsequently completing the octahedral environments around the molybdenum atoms Mo(3) and Mo(4) with terminal and bridging oxygen atoms. The resulting species would, like $[Mo_8O_{27}]^{6-}$, result in a polymeric structure by sharing terminal oxygen atoms.

Table 3 The ESR data for Mn^{2+}(aq) in various aqueous solutions ($[Mn^{2+}]$ = 0.0025 mol dm^{-3}, pH 5.30, room temperature)

	$MnSO_4$ in H_2O	Mn^{2+} + $[MoO_4]^{2-}$ [a,b]	Mn^{2+} in acetate buffer[a]	Mn^{2+} + $[MoO_4]^{2-}$ in acetate buffer[a,b]
g_{av}	2.002	2.002(1)	2.002(1)	2.002(1)
A_{iso}/G	95(1)	95(1)	95(1)	95(1)
Linewidth[c]/G	26(1)	32(1)	34(1)	37(1)
Relative integrated intensity	100[d]	55 ± 10	57 ± 10	52 ± 10

G = 10^{-4} T.

[a] I = 1.00 mol dm^{-3}. [b] Mo:Mn = 25:1. [c] For the $m_I = +\frac{1}{2}$ transition. [d] Defined as 100%.

field splitting, in this case caused by ligand–solvent exchange involving ligand occupation of both the primary and secondary solvation spheres. This corresponds to 'true' complexation (*i.e.* tight binding) and 'ion-pair' formation, respectively. In cases when the formation constants are high, such as ethylenediaminetetraacetate ($edta^{4-}$) (log K_1 = 13.81 at 25 °C and I = 0.1 mol dm^{-3}),[27] no ESR signals have been observed.[28] Static distortion of the ligand field around Mn^{2+} occurs, leading to a large zero-field splitting which, coupled with molecular tumbling, leads to shortened lifetimes for the excited states and a broadened signal which cannot be observed.

The data given in Table 3 for a 0.0025 mol dm^{-3} aqueous solution of $MnSO_4$ at pH 5.3 are typical of that previously reported for $[Mn(OH_2)_6]^{2+}$, indicating little effect on the Mn^{2+}(aq) environment by SO_4^{2-} at the concentration examined. Compared to the integrated intensity of the ESR signal for $[Mn(OH_2)_6]^{2+}$ in solution (*a*), some reduction was observed (*ca.* 40–50%) in the other solutions, indicating the formation of species which are ESR inactive, presumably as a result of occupation of the primary co-ordination sphere and the creation of a zero-field splitting. Reductions in signal intensity have also been observed for the Mn^{2+} signal in acetonitrile and methanol on complexation by Cl^-, Br^-, NCS^-, NO_3^- and ClO_4^-, with losses in intensity of up to 90%, again associated with the formation of species which are ESR inactive.[29,30]

The loss of Mn^{2+} signal intensity on addition of molybdate and/or acetate is not unexpected as all of these solutions have a substantial added anion concentration. However, given the concentration of added anions, all well in excess of the Mn^{2+}(aq) concentration, the actual observation of ESR signals for Mn^{2+} in the presence of molybdate and/or acetate indicates that there are only weak interactions between these anions and Mn^{2+}(aq), that is their respective K_1 values must be relatively small. The g_{av} and A_{iso} values found for Mn^{2+} in these solutions were identical within experimental error to those for $[Mn(OH_2)_6]^{2+}$, but the linewidth of the $m_I = +\frac{1}{2}$ hyperfine signal did show an increase in each case. In the case of acetate, for which K_1 = 4.9 dm^3 mol^{-1} at 25 °C and I = 1.0 mol dm^{-3},[31] the $[MeCO_2^-]$ in our sample was *ca.* 0.5 mol dm^{-3}, which leads to significant 'complexation' of Mn^{2+} in the sample (71%, based on simple equilibrium calculations), probably involving the combined effects of ligand penetration into both the primary and secondary solvation spheres (which presumably K_1 is a total measure of, given the method of its determination, *i.e.* potentiometric titration[32]). Assuming the rate of ion-pair formation is faster than that of ligand substitution into the primary solvation sphere, as is likely, then some broadening of the residual signal for Mn^{2+} is expected to occur as these processes proceed at a rate comparable to the ESR time-scale.[23]

Not surprisingly, the linewidth in the presence of acetate buffer was significantly greater than found for $[Mn(OH_2)_6]^{2+}$. For molybdate, however, the interpretation is complicated by speciation problems. At pH 5.3, 25 °C and at a total $[MoO_4]^{2-}$ concentration of 0.0625 mol dm^{-3} (*i.e.* a Mo:Mn ratio of 25:1), molybdate exists predominantly as a mixture of $[Mo_7O_{24}]^{6-}$ and $[MoO_4]^{2-}$ (see below). Although the individual K_1 values for complexation of Mn^{2+} are unknown, none would appear to be sufficiently high enough to cause complete loss of the ESR signal for Mn^{2+} even though the concentrations of $[MoO_4]^{2-}$ and $[Mo_7O_{24}]^{6-}$ actually in solution are both greater than that of Mn^{2+}. Thus the interactions of these anions with Mn^{2+}(aq) must also be quite weak. The measured linewidth was not as great as observed in the case of acetate, but the lower overall molybdate concentration together with the distribution of molybdenum between numerous species precludes any confident conclusions to be drawn regarding the relative order of interaction of Mn^{2+} with acetate, $[MoO_4]^{2-}$ or isopolymolybdate ions as ligands based on linewidth considerations. The linewidth showed no variation with pH (measurements at pH 4.7 and 4.1) within experimental error, perhaps suggesting that the broadening is caused by interaction with species present in a significant concentration over the entire pH range examined, which suggests that the putative isopolymolybdate species might be $[Mo_7O_{24}]^{6-}$. This would be consistent with the formation and precipitation of $Na_4[MnMo_8O_{27}]\cdot 20H_2O$, as described above, rather than the formation of $[H_6MnMo_6O_{24}]^{4-}$ which would contain effectively Mn^{II} complexed by six (polymerized) molybdate units. Admittedly the molybdenum-containing units are different. However, this is likely associated with a concentration effect, which seems to favour precipitation of $[Mo_8O_{27}]^{6-}$ at high concentrations,[18] while the major isopolymolybdate anion detected in solution is $[Mo_7O_{24}]^{6-}$. In the presence of both molybdate and acetate buffer the linewidth was slightly larger than observed in any of the above solutions. This is probably a reflection of an increased (fluctuating) zero-field splitting caused by species which contain both acetate and molybdate (and/or isopolymolybdate) ligands entering the secondary solvation sphere around $[Mn(OH_2)_6]^{2+}$. The linewidth showed no variation with pH (4.7 and 4.1) within experimental error. It should be noted that the solutions containing both molybdate and acetate buffer are identical in make-up to those used in the kinetic study, as discussed below. The conclusion that may be drawn from the above study is that, given the presence of a significant ESR signal from $[Mn(OH_2)_6]^{2+}$ over the entire pH range investigated in the kinetic study, with evidence for only very weak interaction(s) with the actual molybdate species present, the Mn^{2+} species implicated as the substrate is $[Mn(OH_2)_6]^{2+}$ and not the previously assumed manganese(II) polymolybdate anion, $[H_6MnMo_6O_{24}]^{4-}$, for which no convincing evidence seems to have yet been obtained. The low formation constants evident for complexation of Mn^{II} are, of course, related to the absence of any crystal-field stabilization energy associated with the (high-spin) d^5 electron configuration in an octahedral environment, and this will also have some bearing on why Mn^{2+} does not appear to exist as $[H_6MnMo_6O_{24}]^{4-}$.

Attempts to obtain the ESR spectrum of d^3 Mn^{IV} ($S = \frac{3}{2}$) in $[MnMo_9O_{32}]^{6-}$ in solution were unsuccessful. Although the spectrum at room temperature of Mn^{IV} doped into the isostructural and diamagnetic $[NH_4]_6[NiMo_9O_{32}]\cdot 6H_2O$ has been obtained,[33,34] the site symmetry[9] for Mn^{IV} is C_3 and exhibits a large static zero-field splitting (equal to $2D$, where D = 0.861 cm^{-1}), which presumably leads to fast relaxation and signal broadening.

Oxidation Kinetics of Formation of $[MnMo_9O_{32}]^{6-}$ *with* HOCl *as Oxidant.*—Oxidation of $[Mn(OH_2)_6]^{2+}$ in the presence of molybdate over the range pH 4.0–5.4 using HOCl as oxidant occurs quickly at room temperature and below to give

Table 4 Observed rate constants for oxidation of manganese(II) by hypochlorous acid in the presence of molybdate:oxidant dependence ($[Mn^{2+}] = 0.0025$, $[MoO_4^{2-}] = 0.0625$ mol dm^{-3}, pH 4.49 or 5.36, $I = 1.00$ mol dm^{-3}, 10 °C)

[HOCl]/ mol dm^{-3}	pH	k_{ac}/dm^3 mol^{-1} s^{-1}	$10^5[MnMo_9O_{32}^{6-}]_i$/ mol dm^{-3}	k'_{ac}/ dm^6 mol^{-2} s^{-1}
0.005	4.49	0.17(1)	18.5	75.3
	5.36	2.2(1)	4.5	440
0.010	4.49	0.41(2)	12.0	81.8
	5.36	4.7(2)	3.9	470
0.020	4.49	0.88(4)	9.6	79.1
	5.36	8.8(4)	3.3	440
0.030	4.49	1.39(6)	8.9	78.4
	5.36	14.6(8)	2.1	487
0.040	4.49	1.96(9)	6.8	79.4

Table 5 Observed rate constants for oxidation of manganese(II) by hypochlorous acid in the presence of molybdate: pH dependence ($[Mn^{2+}] = 0.0025$, $[MoO_4^{2-}] = 0.0625$, [HOCl] = 0.030, $I = 1.00$ mol dm^{-3}, 10.0 °C)

pH	k_{ac}/dm^3 mol^{-1} s^{-1}	$10^5[MnMo_9O_{32}^{6-}]_i$/ mol dm^{-3}	$[MoO_4^{2-}]_{calc}$[a]/ mol dm^{-3}
4.03	0.36(2)	11.3	0.000 514
4.49	1.39(6)	8.9	0.001 73
4.67	2.5(1)	8.1	0.002 77
5.05	7.7(4)	3.9	0.007 46
5.36	14.6(8)	2.1	0.016 5
5.70[b]	27.9(14)	2.9	0.037 0

[a] From data in refs. 36 and 37. [b] Only 70% conversion under autocatalytic conditions.

Table 6 Observed rate constants for oxidation of manganese(II) by hypochlorous acid in the presence of molybdate: molybdate dependence ($[Mn^{2+}] = 0.0010$, [HOCl] = 0.020, $I = 2.50$ mol dm^{-3}, 10.0 °C)

Total $[MoO_4^{2-}]$/ mol dm^{-3}	pH	k_{ac}/ dm^3 mol^{-1} s^{-1}	$10^5[MnMo_9O_{32}^{6-}]_i$/ mol dm^{-3}	$[MoO_4^{2-}]_{calc}$*/ mol dm^{-3}
0.0125	5.07	1.25(6)	14.3	0.005 79
0.0250	5.13	2.4(1)	10.1	0.007 79
0.0500	5.20	4.5(2)	6.3	0.010 6
0.1000	5.30	8.4(4)	2.1	0.015 3

* From data in refs. 36 and 37.

$[MnMo_9O_{32}]^{6-}$. The pH range is rather narrow, but this is a limitation placed on the study by the range of stability reported for the product species.[7] Based on the known molar absorptivity of $[MnMo_9O_{32}]^{6-}$, complete conversion into this species occurred under the range of experimental conditions employed in this study. With the exception of a temperature-dependence study, all oxidation kinetics were subsequently monitored at 10 °C.

A typical absorbance–time trace for the formation of $[MnMo_9O_{32}]^{6-}$ is shown in Fig. 2. The trace exhibits the S-shaped curve for an autocatalytic reaction. In view of the known heterogeneous autocatalytic effect of MnO_2 on Mn^{2+} oxidation, attempts were therefore made to identify this species during the course of reaction. Thus, for example, continuous monitoring of the UV/VIS spectrum between 700 and 350 nm over the course of a typical oxidation reaction showed only the absorption bands attributable to $[MnMo_9O_{32}]^{6-}$, with no evidence of any intermediate species or formation of particulate matter (MnO_2), which may be monitored at 500 nm.[4] There is, therefore, no evidence that MnO_2 plays any part in the mechanism of $[MnMo_9O_{32}]^{6-}$ formation in this reaction.

The kinetic data were consequently analysed in terms of a

Table 7 Observed rate constants for oxidation of manganese(II) by hypochlorous acid in the presence of molybdate:temperature dependence ($[Mn^{2+}] = 0.0025$, total $[MoO_4^{2-}] = 0.0625$, [HOCl] = 0.020 mol dm^{-3}, pH 5.36, $[MoO_4^{2-}]_{calc} = 0.0165$ mol dm^{-3}, $I = 1.00$ mol dm^{-3})

T/°C	k_{ac}/dm^3 mol^{-1} s^{-1}	$10^5[MnMo_9O_{32}^{6-}]_i$/ mol dm^{-3}
4.8	4.4(2)	4.3
10.0	8.8(4)	3.3
13.0	11.3(5)	2.9
15.0	13.3(7)	2.4
17.5	16.1(8)	2.0
20.0	18.9(9)	1.9

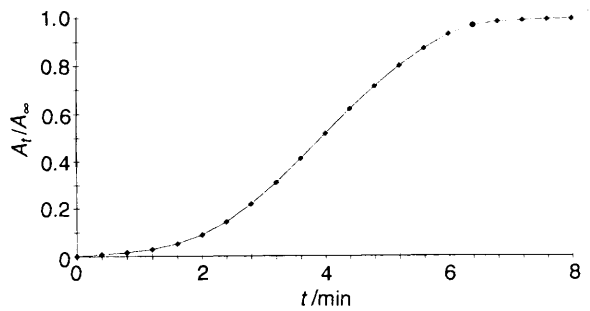

Fig. 2 Typical autocatalysis curve for the oxidation of Mn^{2+}(aq) by HOCl in weakly acidic solution in the presence of molybdate. $[Mn^{2+}] = 0.0025$, [HOCl] = 0.030, $[MoO_4^{2-}] = 0.0625$ mol dm^{-3}, pH 5.05, $I = 1.00$ mol dm^{-3}, 10.0 °C

second-order autocatalytic reaction which obeyed rate law (3) where k_{ac} is a pseudo-second-order rate constant, which

$$+d[MnMo_9O_{32}^{6-}]/dt = k_{ac}[Mn^{2+}][MnMo_9O_{32}^{6-}] \quad (3)$$

subsumes dependences on [HOCl] and, as shall be shown below, $[MoO_4^{2-}]$ and $[HMoO_4^-]$. Following the standard treatment for second-order autocatalysis (see, for example, ref. 35), a plot of $\ln[(A_t/A_\infty)/(1 - A_t/A_\infty)]$ against time gives a straight line of slope $k_{ac}[Mn^{2+}]_i$, where $[Mn^{2+}]_i$ is the initial concentration of Mn^{2+} and, from the intercept (y) on the ordinate axis, a measure of the 'initial' product concentration, $[MnMo_9O_{32}^{6-}]_i$, which is 'instantaneously' formed on mixing the two solutions containing the starting reagents ($[MnMo_9O_{32}^{6-}]_i = [Mn^{2+}]_i e^y$). A list of rate constants and $[MnMo_9O_{32}^{6-}]_i$ values obtained under various conditions are given in Tables 4–7.

The autocatalytic rate constant k_{ac} shows a first-order dependence on [HOCl] at a pH of 5.36 but surprisingly exhibits a slight deviation from first-order behaviour under kinetically slower reaction conditions at a pH of 4.49. For both, a plot of log k_{ac} against log[HOCl] gives a straight line, with slopes of 1.03(4) ($R^2 = 0.9974$) at pH 5.36 and 1.16(2) ($R^2 = 0.9992$) at pH 4.49, allowing the expanded rate expression (4) (at pH

$$+d[MnMo_9O_{32}^{6-}]/dt = k'_{ac}[Mn^{2+}][MnMo_9O_{32}^{6-}][HOCl] \quad (4)$$

5.36). The deviation from first-order behaviour at pH 4.49 is outside the limits of error in the data even when the error in k_{ac} is considered (minimum and maximum slopes of 1.12 and 1.22, respectively). Notably, a similar deviation from first-order dependence has previously been observed at a pH of 4.54 for the oxidation of Mn^{2+} in the presence of molybdate using HSO_5^-.[8] As Mn^{II} is almost certainly oxidized to Mn^{IV} through a manganese(III) intermediate, the departure from first-order behaviour at this pH may well be a reflection of the participation of two molecules of HOCl in the oxidation process by an

alternative pathway, which only emerges at lower pH values (see also below).

In order to determine the potential dependences of the rate on $[H^+]$ and molybdate concentrations, the variations of k_{ac} with both pH and total added $[MoO_4^{2-}]$ were examined. The variation with pH appears complex (Fig. 3), while, at a pH of *ca.* 5.2, k_{ac} shows a non-linear relationship with total added $[MoO_4^{2-}]$ [Fig. 4(*a*)]. The behaviour in both cases is tied to the changes in speciation of molybdate with both pH and concentration. The only such investigations currently available have been performed at 25 °C in 3 mol dm^{-3} $NaClO_4$.[36-38] While it is to be appreciated that the present study was carried out at 10 °C and I = 1.00 (pH dependence) or 2.50 mol dm^{-3} ($[MoO_4^{2-}]$ dependence), the differences in conditions are not so great that the general trends observed in the speciation studies are not applicable to this work. This is also addressed below. In our previous studies the observed pH dependence was attributed to a protonation–deprotonation equilibrium involving a manganese(II) or nickel(II) heteropolymolybdate present in solution prior to introduction of the oxidant. Clearly this is not the case in the present study as the ESR investigation has established that manganese(II) exists effectively as $[Mn(OH_2)_6]^{2+}$ over the entire pH range examined. Furthermore, HOCl acts as an oxidant in acidic, neutral and basic solution (the latter as OCl^-; pK_a = 7.53 at 25 °C[39]) and would be fully protonated over the pH range examined. Also, k_{ac} actually decreases with *increasing* $[H^+]$. It is therefore proposed that as a first approximation there is no real dependence on $[H^+]$, but that the observed trend of k_{ac} with pH is primarily caused through an actual change in molybdate speciation. Over the pH range examined (4.03–5.36), at a total added $[MoO_4^{2-}]$ of 0.0625 mol dm^{-3}, the molybdate species in solution are predominantly $[Mo_7O_{24}]^{6-}$ and $[MoO_4]^{2-}$ and, to a lesser extent, their protonated forms $[HMo_7O_{24}]^{5-}$, $[HMoO_4]^-$ and H_2MoO_4. Using the formation constants calculated by Ozeki *et al.*[36,37] for these five species, the concentrations of $[HMo_7O_{24}]^{5-}$ and H_2MoO_4 are both found to decrease with increasing pH, while $[Mo_7O_{24}]^{6-}$ increases until a pH of 4.40–4.41, after which it decreases. Thus these three species may be discounted as the cause of the observed trend in k_{ac}. Of the remaining two species, $[MoO_4]^{2-}$ and $[HMoO_4]^-$, the one that exhibits a concentration profile closest to that of the trend in k_{ac} is $[MoO_4]^{2-}$. The concentration of $[MoO_4]^{2-}$ actually present in solution (*i.e.* $[MoO_4^{2-}]_{calc}$, see Table 5) increases by a factor of 32 from pH 4.03 to 5.36, while that of $[HMoO_4]^-$ increases by only 1.5 (2.85 × 10^{-4} to 4.26 × 10^{-4} mol dm^{-3}). Over the same pH range, k_{ac} increases by a factor of 40. Moreover, a measurement of k_{ac} at a pH of 5.70, although formally outside of the reported range of stability of $[MnMo_9O_{32}]^{6-}$, gave a value of 27.9 dm^3 mol^{-1} s^{-1}, implying that the dependence on $[MoO_4^{2-}]$ is still increasing dramatically above pH 5.36, as does $[MoO_4^{2-}]_{calc}$ (Table 5). Thus, a plot of k_{ac} against $[MoO_4^{2-}]_{calc}$ produces an approximately linear relationship indicating some dependence of k_{ac} on the actual concentration of $[MoO_4]^{2-}$ in solution. The observed non-linearity might be attributable to the use of $[MoO_4^{2-}]_{calc}$ values taken from formation constants measured at a different temperature and ionic strength, as indicated above, and would reflect differences in the polymerization of molybdate under the two sets of experimental conditions. Alternatively, the trend in k_{ac} may also involve a real dependence on $[H^+]$ in addition to the dependence on $[MoO_4^{2-}]$. These possibilities are resolved below.

For the molybdate dependence study, over the range of concentrations examined (0.0125–0.100 mol dm^{-3}), the major species in solution are $[Mo_7O_{24}]^{6-}$ and $[MoO_4]^{2-}$, with considerably lower concentrations of the other three species. In this study, however, even with the increased buffering capacity used to allow an extensive range of Mo:Mn ratios under pseudo-second-order autocatalytic conditions (Mo:Mn > 5), some slight variations in pH were noted (ΔpH 0.23 over the

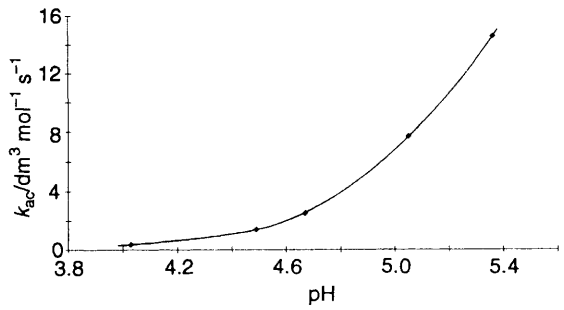

Fig. 3 Dependence of k_{ac} on pH. $[Mn^{2+}]$ = 0.0025, [HOCl] = 0.030, $[MoO_4^{2-}]$ = 0.0625, I = 1.00 mol dm^{-3}, 10.0 °C

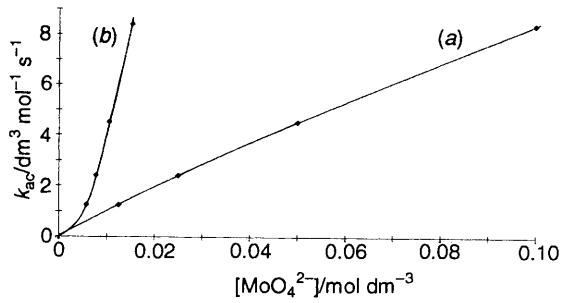

Fig. 4 Dependence of k_{ac} on total added molybdate (*a*) and on actual $[MoO_4^{2-}]$ (*b*) in solution. $[Mn^{2+}]$ = 0.0010, [HOCl] = 0.020, I = 2.50 mol dm^{-3}, 10.0 °C

range of total $[MoO_4]^{2-}$ concentrations employed). Not surprisingly, if k_{ac} is plotted against the total added $[MoO_4^{2-}]$ [Fig. 4(*a*)] then a non-linear relationship is obtained. However, if k_{ac} is plotted against $[MoO_4^{2-}]_{calc}$ then the upper curve [Fig. 4(*b*)] is obtained, which suggests a higher-than-first-order dependence. Now, assuming that the differences in molybdate polymerization under the experimental conditions of this study and those employed in the estimation of the formation constants are not great (see also below), then the $[MoO_4^{2-}]_{calc}$ values may be used to establish the actual molybdate dependence. Significantly, a plot of log k_{ac} against log-$[MoO_4^{2-}]_{calc}$ produces a linear relationship (R^2 = 0.9958) with a slope of 1.96(9), which indicates a second-order dependence on $[MoO_4^{2-}]$.

If the second-order dependence on $[MoO_4^{2-}]$ is now included in the rate expression above, this can be written as in equation (5) where k''_{ac} is 1.79(18) × 10^6 dm^{12} mol^{-4} s^{-1} at

$$+d[MnMo_9O_{32}^{6-}]/dt = k''_{ac}[Mn^{2+}][MnMo_9O_{32}^{6-}][HOCl][MoO_4^{2-}]^2 \quad (5)$$

10 °C based on the actual $[MoO_4^{2-}]$ present in solution at a pH of 5.36 as calculated from the reported formation constants. This value has an estimated error of *ca.* ± 10%, but is perhaps even greater given that ionic strength effects have not been included in the estimation of k''_{ac}.

With the dependence of k_{ac} on $[MoO_4^{2-}]$ now established, it is possible to return to the trend in k_{ac} with pH, remove the $[MoO_4^{2-}]$ dependence, and investigate the possibility of an actual dependence on $[H^+]$. A plot of $\log\{k_{ac}/([MoO_4^{2-}]_{calc})^2\}$ against $\log[H^+]$ provides a linear relationship of slope 1.04(4) (R^2 = 0.9958), indicating a first-order dependence on $[H^+]$. Thus the rate expression may be further expanded to include this dependence, equation (6) where k'''_{ac} is 4.8(5) × 10^{11}

$$+d[MnMo_9O_{32}^{6-}]/dt = k'''_{ac}[Mn^{2+}][MnMo_9O_{32}^{6-}][H^+][HOCl][MoO_4^{2-}]^2 \quad (6)$$

dm^{15} mol^{-5} s^{-1} at 10 °C. This value is an average over the three highest pH values (4.67–5.36), below which the

dependence on [HOCl] becomes non-linear. An alternative form of this rate expression would involve the combination of the dependences on $[H^+]$ and on $[MoO_4^{2-}]$ through the protonation reaction $H^+ + [MoO_4]^{2-} \longrightarrow [HMoO_4]^-$ (for which $\log \beta = 3.773$).[37] This, in turn leads to a rate expression of the form (7) where $k_{AC} = 8.1(9) \times 10^7$ dm^{12} mol^{-4} s^{-1} at

$$+d[MnMo_9O_{32}^{6-}]/dt = k_{AC}[Mn^{2+}][MnMo_9O_{32}^{6-}][HOCl][MoO_4^{2-}][HMoO_4^-] \quad (7)$$

10 °C. The expression is not unrealistic as it simply involves the important molybdate species $[MoO_4]^{2-}$ and $[HMoO_4]^-$ in addition to oxidant (HOCl), substrate (Mn^{2+}) and, as required in an autocatalytic process, product ($[MnMo_9O_{32}]^{6-}$).

At this point some comments should be made on the variation in polymerization involving the difference in experimental conditions employed for the measurement of the formation constants and those used in this study. If it is assumed that the Arrhenius activation energy (E_a) remains constant with temperature for this system, then any variation in slope of the plot of ln k_{ac} against $1/T$ may be attributed to a change in the actual $[MoO_4^{2-}]$ in solution, that is to a change in polymerization with temperature, provided all other conditions remain constant. The data (at pH 5.36) are given in Table 7. Notably, the plot is not linear and E_a varies from *ca.* 95 to 40 kJ mol^{-1}, decreasing as the temperature increases over the range studied, with an average $E_a = 68$ kJ mol^{-1} ($R^2 = 0.981$). However, in view of the complexity of the reaction mechanism, the (effective) activation energy that can be calculated merely represents an 'average' value for the overall series of reactions contributing to the mechanism. More importantly, however, following the assumption that E_a is constant, the observation of a non-linear Arrhenius relationship indicates that the effective concentration of $[MoO_4]^{2-}$ does not remain constant over the temperature range employed. This is a reflection of the changing speciation of molybdate with temperature. Based on the observed *trend* of E_a with temperature and consequently k_{ac}, and, in turn, $[MoO_4^{2-}]$, it can be concluded that there is increased polymerization at lower temperatures. Using a value of k_{ac} calculated assuming constant E_a (40 kJ mol^{-1} at 25 °C) compared to the value actually obtained at 10 °C, the decrease in the actual $[MoO_4^{2-}]$ is only *ca.* 8%, which supports the use of concentrations calculated from the formation constants obtained at the higher temperature. A value for k_{AC} at 25 °C of $1.36(10) \times 10^8$ dm^{12} mol^{-4} s^{-1} may be estimated from an extrapolated value of k_{ac} at this temperature (24.5 dm^3 mol^{-1} s^{-1}) based on the Arrhenius plot, along with the actual $[MoO_4^{2-}]$ present in solution according to the reported formation constants (actually obtained at 25 °C).

Mechanistic Considerations.—With the rate-determining step established above, some considerations concerning the possible mechanism of this reaction can be proposed. The mechanism of oxidation of Mn^{2+}(aq) by HOCl in the presence of molybdate to give $[MnMo_9O_{32}]^{6-}$ can be expressed as in equations (8)–(10) where the involvement of molybdate as $[MoO_4]^{2-}$,

$$Mn^{2+} \xrightarrow[HOCl]{k_1} Mn^{3+} \quad (8)$$

$$Mn^{3+} + Mn^{3+} \xrightarrow[HOCl]{k_2} 2Mn^{4+} \quad (9)$$

$$Mn^{2+} + Mn^{4+} \underset{k_{-3}}{\overset{k_3}{\rightleftharpoons}} 2Mn^{3+} \quad (10)$$

$[HMoO_4]^-$ or any isopolymolybdate is currently unknown, and HOCl is involved in the two oxidation steps. The third step, expressed as a competition between k_3 and k_{-3}, is required to create the observed autocatalysis. Owing to our lack of knowledge surrounding the molybdate balance in the above equations, they simply follow the fate of manganese in the proposed mechanism and, as such, the rate equations which describe the above steps involve pseudo-first or second-order rate constants. This sequence of steps is consistent with HOCl acting as a one- or two-electron oxidant as shown by equations (11) and (12). As the rate-determining step [equation (7)] contains a

$$HOCl + H^+ + e^- \longrightarrow \tfrac{1}{2}Cl_2 + H_2O \quad (11)$$

$$HOCl + H^+ + 2e^- \longrightarrow Cl^- + H_2O \quad (12)$$

term in oxidant, one of the oxidation steps must be the limiting stage. Moreover, assuming the forward and reverse rate constants that govern equilibrium (10) are both greater than that governing the rate-determining step, then the dependences on $[Mn^{2+}]$ and $[Mn^{4+}]$ in the rate-determining step can be replaced by $[Mn^{3+}]^2$ (with inclusion of the equilibrium constant), making oxidation of Mn^{3+} the limiting stage and, moreover, second order in $[Mn^{3+}]$. This is indicated in the above scheme. This step would also have to be the dominant term in the expression describing the overall rate of formation of $[MnMo_9O_{32}]^{6-}$. The oxidant, HOCl, is presumably acting as a two-electron oxidant (to two Mn^{3+}) in this reaction. Notably, the deviation from first-order dependence on [HOCl] observed at lower pH (4.49) is likely a reflection of two-electron involvement in this step, but favouring the involvement of two single HOCl molecules, now acting as one-electron oxidants, under the more acidic and kinetically slower reaction conditions. A likely transition state would therefore consist of two Mn^{3+} ions {each with a partial polymolybdate environment already in place as a result of molybdate involvement in the first step [equation (8)]}, linked by bridging $[MoO_4]^{2-}$ and $[HMoO_4]^-$ ions, together with a co-ordinated HOCl molecule.

Using the above set of four rate equations as a basis, two models were investigated involving some or all of the steps by refining the rate constants for the particular model to a set of experimental data using a numerical-integration enhanced curve-fitting program.[40] The set of experimental data chosen was $[Mn^{2+}] = 0.0025$ mol dm^{-3}, total $[MoO_4^{2-}] = 0.0625$ mol dm^{-3}, pH 5.05 (giving $[MoO_4^{2-}]_{calc} = 0.007\,46$ mol dm^{-3} and $[HMoO_4^-] = 0.000\,394$ mol dm^{-3}, *i.e.* Mo:Mn ratios of 3.0 and 0.16, respectively), [HOCl] = 0.030 mol dm^{-3} and temperature = 10.0 °C. This is actually the absorbance–time trace shown in Fig. 2. The criteria that may be used to assess these models were based on the following chemical observations. First, as indicated above, continuous UV/VIS spectral monitoring of a typical reaction showed no evidence for any intermediate during the formation of $[MnMo_9O_{32}]^{6-}$ and, secondly, equilibrium (10) must favour Mn^{2+} and Mn^{4+} (*i.e.* $k_{-3} > k_3$). This is supported by two observations. The ESR spectrum of the solution formed by combining equal volumes of one containing Mn^{2+} and MoO_4^{2-} ($[Mn^{2+}] = 0.0025$, $[MoO_4^{2-}] = 0.0625$ mol dm^{-3}) and one containing $[NH_4]_6[MnMo_9O_{32}]$ ($[Mn^{4+}] = 0.0025$ mol dm^{-3}), both in acetate buffer at pH 5.3 ($I = 1.0$ mol dm^{-3}), showed no decrease in integrated intensity of the Mn^{2+} signal other than that caused by simple two-fold dilution. Also, addition of 'manganese(III) acetate dihydrate', which probably contains $[Mn_3O(MeCO_2)_6(OH_2)_3]^+$,[41] in 5 mol dm^{-3} H_2SO_4 to an acetate buffer solution at pH 5.3 containing an excess (25:1) of $Na_2[MoO_4]$ quickly gave a red-brown solution which was shown to contain $[MnMo_9O_{32}]^{6-}$ by UV/VIS spectroscopy. (There was no evidence for the formation of solid MnO_2 in this reaction.) Thus the equilibrium step (10) has been approached from both sides with consistent results.

The first model included just three rate constants, k_1, k_2 and k_3, and gave values of 2.63×10^{-3} s^{-1}, 8.48 dm^3 mol^{-1} s^{-1} and 14.43 dm^3 mol^{-1} s^{-1}, respectively. While the fit to the absorbance–time trace was quite good, a significant build-up in $[Mn^{3+}]$ (40% of the initial $[Mn^{2+}]$) occurred in the middle stages of the calculated species distribution–time profile, which is contrary to the above expectations. This results simply as no

account of the disproportionation of Mn^{3+} into Mn^{2+} and Mn^{4+} has been included in the calculation. Incorporation of k_{-3} leads to the second model. However, it was found that not all four rate constants could be independently evaluated, so that some alternative means of establishing one or more of the values was required to obtain the rate constants. Some feel for the equilibrium between k_3 and k_{-3} can be gained from the disproportionation of Mn^{3+} in weakly acidic aqueous solution to give Mn^{2+} and MnO_2 according to the equation $2Mn^{3+} + 2H_2O \longrightarrow Mn^{2+} + MnO_2(s) + 4H^+$, for which the equilibrium constant is $\approx 2 \times 10^9$ based on electrochemical data.* As the disproportionation is to a large extent driven by the insolubility of MnO_2, this value of K represents an extreme upper limit to the equilibrium constant which is defined by k_3 and k_{-3} in that it is large, although the above value by its very nature and the way it was obtained can only represent a very approximate value in this case, especially in the presence of added molybdate. Indeed, some stability of Mn^{3+} is gained on complexation, such as in $[Mn(C_2O_4)_3]^{3-}$ and $[Mn(acac)_3]$ (acac = acetylacetonate), but decomposition occurs with time, usually involving oxidation of the ligand. This is not possible in the case of polymolybdate as the ligand. The value of K is therefore likely to be considerably less than that given above. Consequently, K (*i.e.* k_{-3}/k_3) was varied between 1 and 2×10^9 by allowing the three rate constants k_1, k_2 and k_3 to refine for various values of k_{-3}. This gave values of 8.01×10^{-4} s^{-1}, 216 dm^3 mol^{-1} s^{-1}, 232 dm^3 mol^{-1} s^{-1} and 6.67×10^3 dm^3 mol^{-1} s^{-1} for k_1, k_2, k_3 and k_{-3}, respectively, as the only realistic choice of rate constants. The equilibrium constant K is only 29, which is considerably less than the maximum value estimated above, and reflects the stabilization of Mn^{III} in a polymerized molybdate environment. The rate constants are able to reproduce the absorbance–time trace almost perfectly and somewhat better than in the previous model. Importantly, there is much reduced presence (6%) of Mn^{III} during the middle stages of the calculated species distribution–time profile. Attempts to reduce k_3 and k_{-3} relative to the other rate constants resulted in incomplete reaction and a significant Mn^{3+} presence in the species distribution–time profile, while increasing these rate constants did not produce a solution to the rate equations. These rate constants can now be used to calculate the previously obtained autocatalytic rate constant k_{ac} (a pseudo-second-order rate constant), as defined in equation (3), for this particular set of reaction conditions. Substitution of the equilibrium expression from (10) in the equation describing the overall rate of formation of $[MnMo_9O_{32}]^{6-}$ gives that derived from equation (9) as the only effective term, so that $d[MnMo_9O_{32}{}^{6-}]/dt = (k_2/K)[Mn^{2+}][MnMo_9O_{32}{}^{6-}]$. The autocatalytic rate constant k_{ac} should therefore equal k_2/K (*i.e.* k_2k_3/k_{-3}), or 7.5 dm^3 mol^{-1} s^{-1}. This value is in good agreement with the value of 7.7(4) dm^3 mol^{-1} s^{-1} determined (see Table 5).

Acknowledgements

We thank Dr. M. Maeder for access to his modelling program and for discussions on its application to reaction mechanisms. The Universities of Sydney and New South Wales are also acknowledged for providing access to the Bruker ESP300 spectrometer.

* This value of K may be derived from the standard reduction potentials of Mn^{3+}–Mn^{2+} (+1.5 V) and MnO_2, H^+–Mn^{3+}, H_2O (+0.95 V), using the Nernst equation.

References

1 W. Stumm and J. J. Morgan, *Aquatic Chemistry*, Wiley-Interscience, New York, 1970.
2 D. E. Wilson, *Geochim. Cosmochim. Acta*, 1980, **44**, 1311.
3 D. A. House, *Chem. Rev.*, 1962, **62**, 185.
4 G. A. Lawrance and C. B. Ward, *Transition Met. Chem.*, 1985, **10**, 258.
5 Ya. D. Tiginyanu, A. P. Moravskii, V. F. Shuvalov and V. M. Bernikov, *Kinet. Katal. (Engl. Transl.)*, 1983, **24**, 5.
6 P. Souchay and R. Schaal, *Anal. Chim. Acta*, 1949, **3**, 1.
7 L. C. W. Baker and T. J. R. Weakley, *J. Inorg. Nucl. Chem.*, 1966, **28**, 447.
8 S. J. Dunne, R. C. Burns, T. W. Hambley and G. A. Lawrance, *Aust. J. Chem.*, 1992, **45**, 685.
9 S. J. Dunne, R. C. Burns and G. A. Lawrance, *Aust. J. Chem.*, 1992, **45**, 1943.
10 A. La Ginestra, F. Giannetta and P. Fiorucci, *Gazz. Chim. Ital.*, 1968, **98**, 1197.
11 *International Tables for X-Ray Crystallography*, eds. J. A. Ibers and W. C. Hamilton, Kynoch Press, Birmingham, 1974, vol. 4.
12 P. Main, MULTAN 80, University of York, 1980.
13 W. R. Busing, K. O. Martin and H. A. Levy, ORFLS, Oak Ridge National Laboratories, Oak Ridge, TN, 1962.
14 C. K. Johnson, ORTEP II, A Thermal Ellipsoid Plotting Program, Oak Ridge National Laboratories, Oak Ridge, TN, 1976.
15 M. Isobe, F. Marumo, T. Yamase and T. Ikawa, *Acta Crystallogr., Sect. B*, 1978, **34**, 2728.
16 R. D. Adams, W. G. Klemperer and R.-S. Liu, *J. Chem. Soc., Chem. Commun.*, 1979, 256.
17 J. Fuchs, H. Hartl, W.-D. Hunnius and S. Mahjour, *Angew. Chem., Int. Ed. Engl.*, 1975, **14**, 644.
18 V. I. Boschen, B. Buss and B. Krebs, *Acta Crystallogr., Sect. B*, 1974, **30**, 48.
19 A. Zalkin, J. D. Forrester and D. H. Templeton, *Inorg. Chem.*, 1964, **3**, 529.
20 B. Morosin and E. J. Graeber, *J. Chem. Phys.*, 1965, **42**, 898.
21 M. T. Pope, *Heteropoly and Isopoly Oxometallates*, Springer, Berlin, 1983.
22 F. K. Hurd, M. Sachs and W. D. Hershberger, *Phys. Rev.*, 1954, **93**, 373.
23 R. G. Hayes and R. J. Myers, *J. Chem. Phys.*, 1964, **40**, 877.
24 B. B. Garrett and L. O. Morgan, *J. Chem. Phys.*, 1966, **44**, 890.
25 N. Bloembergen and L. O. Morgan, *J. Chem. Phys.*, 1961, **34**, 842.
26 *Critical Stability Constants*, eds. A. E. Martell and R. M. Smith, Plenum, New York, 1982, First Supplement, vol. 5.
27 *Critical Stability Constants*, eds. A. E. Martell and R. M. Smith, Plenum, New York, 1974, vol. 1.
28 M. Cohn and J. Townsend, *Nature (London)*, 1954, **173**, 1090.
29 S. I. Chan, B. M. Fung and H. Lütje, *J. Chem. Phys.*, 1967, **47**, 2121.
30 H. Levanon and Z. Luz, *J. Chem. Phys.*, 1968, **49**, 2031.
31 *Critical Stability Constants*, eds. R. M. Smith and A. E. Martell, Plenum, New York, 1989, Second Supplement, vol. 6.
32 P. W. Linder, R. G. Torrington and U. A. Seeman, *Talanta*, 1983, **30**, 295.
33 C. R. Byfleet, W. C. Lin and C. A. McDowell, *Mol. Phys.*, 1970, **18**, 363.
34 P. G. Rassmussen, K. M. Beem and E. J. Hornyak, *J. Chem. Phys.*, 1969, **50**, 3647.
35 N. M. Emanuel' and D. G. Knorre, *Chemical Kinetics (Homogeneous Reactions)*, Wiley, New York, 1973, p. 271.
36 T. Ozeki, H. Kihara and S. Hikime, *Anal. Chem.*, 1987, **59**, 945.
37 T. Ozeki, H. Kihara and S. Ikeda, *Anal. Chem.*, 1988, **60**, 2055.
38 K. H. Tytko, G. Baethe, E. R. Hirschfeld, K. Mehmke and D. Stellhorn, *Z. Anorg. Allg. Chem.*, 1983, **503**, 43.
39 *Critical Stability Constants*, eds. R. M. Smith and A. E. Martell, Plenum, New York, 1976, vol. 4.
40 M. Maeder and A. D. Zuberbuhler, *Anal. Chem.*, 1990, **62**, 2220.
41 B. Chiswell, E. D. McKenzie and L. Lindoy, *Comprehensive Coordination Chemistry*, eds. G. Wilkinson, R. D. Gillard and J. A. McCleverty, Pergamon, Oxford, 1987, vol. 4, ch. 41, p. 88.

Received 9th *February* 1993; *Paper* 3/00776F